CURRENT-VOLTAGE CHARACTERSTICS AND IMPEDANCE SPECTROSCOPY OF POLY (3-(4′-(1″, 4″), 7″-TRIOXAOCTYL) PHENYL) THIOPHENE) (PEOPT)

A thesis presented to the
School of Graduate Studies
Addis Ababa University

In Partial Fulfillment
of the Requirements for the Degree
of Master of Science in Physics

By
Tesfaye Ayalew

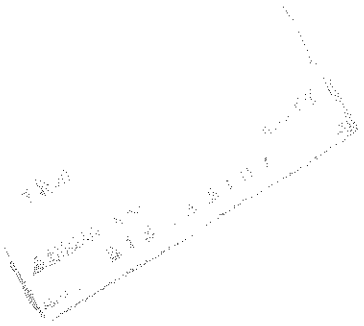

June 2000
Addis Ababa

ACKNOWLEDGEMENT

I have a high debt of gratitude to my advisor, Dr. Bantikassegn workalemahu, for introducing me to the field of conjugated polymer, excellent guidance, encouragement, and material support. The convenient working environment with well-equipped laboratory he has created with the necessary journals and materials are greatly acknowledged.

My sincere thanks also goes to the department of physics, Addis Ababa University.

I would like to express my sincere thanks to the International Program in the Physical Sciences (IPPS) for equipping a research laboratory with all the necessary materials.

I would like to express my gratitude to the German Academic Exchange Service (DAAD) for the financial support throughout my study.

Abstract

This thesis is based on the study of the electronic properties of PEOPT in the form of Al/PEOPT/ITO sandwich structure. An interface between aluminum contacts to PEOPT films were studied using complex impedance spectroscopy and current-voltage characteristic measurements. The current density-voltage curve is asymmetric and non-ohmic and shows Schottky barrier type rectification. The complex impedance spectra are semi-circles that show the existence of a region depleted of mobile charge carriers. An equivalent circuit consisting of one parallel RC circuit is envisaged as a model of the interface.

CONTENTS

List of Figures page

List of Tables

Page

1. INTRODUCTION

Polymers are long-chain organic molecules of very high molecular weight often measured in hundreds of thousands of molar weight. Therefore, these molecules are called macromolecules. While the exact molecular weight that is required for an organic molecule to be called a polymer is a subject of continued debate, often polymer scientists put the number above 25,000-g/mol [1]. This is the minimum molecular weight required for good physical and mechanical properties for many important polymers. The molecular weight is also near the onset of entanglement.

Polymers are insulators or at best semiconductors when chemically pure. Only after treatment with oxidizing (electron accepting) or reducing (electron donating) agents, called 'doping', they become conducting, i.e., doping of polymers creates allowed states in the band gap through which the charge carriers transit. In inorganic semiconductors, doping involves replacing some of the atoms of the semiconductor with atoms that have either more or less electrons while in conducting polymers the dopant molecules never replace any of the atoms of the polymer; rather they simply act as associates that accept or donate electrons [2].

Conjugated polymers are organic semiconductors, the semiconducting behavior being associated with the π molecular orbitals delocalized along the polymer chain. During the last few years the semiconducting properties of conjugated polymers have been the subject of intensive study because of their

potential applications in electronics and optoelectronics. They are considered as alternatives to existing materials because of the ease of device fabrication and their comparatively low cost.

Most conjugated polymers consist of hetrocyclic polymers such as polythiophene and its derivatives. Syntheses of a large number of derivatives of polythiophene with different degrees of stability, conductivity, solubility, and band gap have been possible by addition of side chains to the thiophene ring. Introducing side groups at the 3- and/or 4- positions of the thiophene ring can modify its chemical and physical properties. Among the substituted polythiophenes, poly(3,4-ethylenedioxythiophene), PEDOT, poly(3-octylphenylthiophene), POPT & poly[3-(4-octylphenyl)-2,2′-bithiophene], PTOPT, have been studied. These polythiophene derivatives and other polymers have been tested for their possible applications in electronic and optoelectronic devices such as Schottky junction diodes [3-5], light emitting diodes [6-11], field effect transistors [12,13], and all-solid-state photoelectrochemical cells [14,15]. In all these proposed applications, the nature of the metallic contact to the polymer is of great importance.

In this research work we studied the electrical properties of junctions between aluminium and poly(3-(4′-(1″,4″),7″-trioxaoctyl)phenyl)thiophene), PEOPT, which is another polythiophene derivative. The sandwich structure that we made locally, with which the work has been done, is of the form Al/PEOPT/ITO diode. The current-voltage measurements as well as the complex impedance spectroscopy are used for characterization of this structure. We used thermionic

emission theory to interpret the J-V characteristic and the complex impedance is measured and plotted as a Cole-Cole plot and analyzed.

2. Conjugated polymers

2.1 Conducting polymers

In 1977 it was first discovered that the conductivity of polyacetylene could be increased by chemical oxidation by many orders of magnitude [16,17]. Since then, it has remained a subject of intensive research and debate in international conferences of science and technology of synthetic metals.

There are many reasons for the popularity of conducting polymers. Among these are their promising potential for new applications, the extended systems of conjugated bonds are subjected to quantum mechanical analysis, the existence of solitons and solitary waves creates an interdisciplinary link to field theory and elementary particle physics.

Organic molecules that contain double bonds show different electronic properties compared to saturated molecules, which only have single bonds. Especially in the case of alternating single and double bonds, called conjugation, the polymers manifest properties of technological interest.

The basic chemical structures of some of the most important conducting polymers are shown in Fig.2.1.

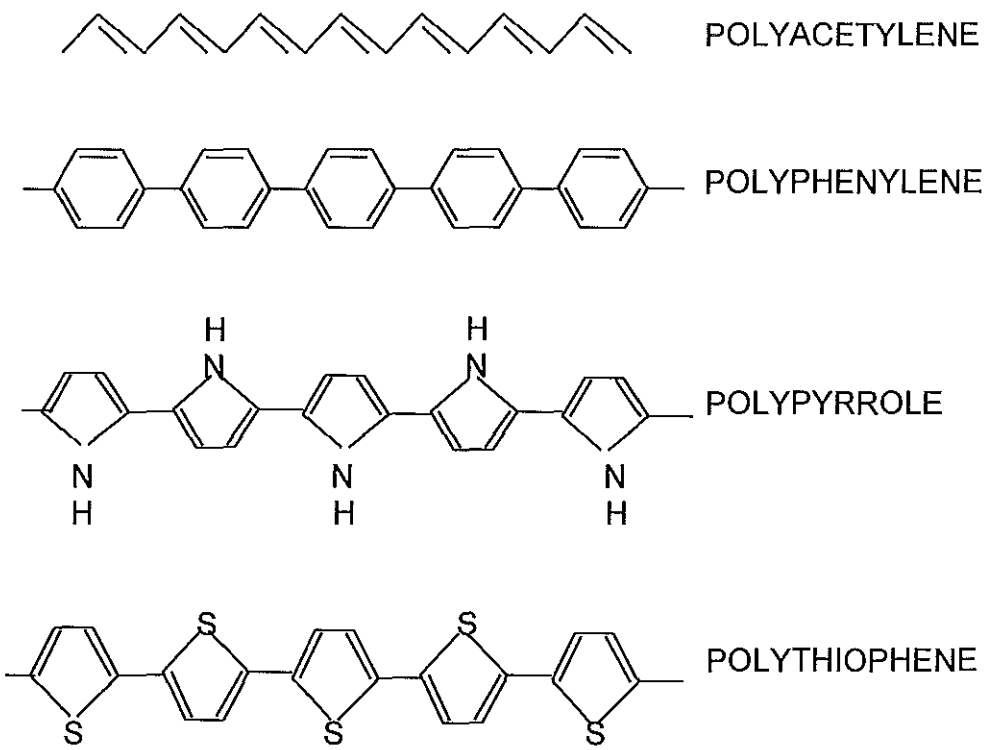

Fig. 2.1 Basic chemical structures of some of the conjugated polymers.

2.2 Hybridization of carbon

The formation of a covalent bond involves the sharing of any two electrons, i.e., the pair that can be accommodated in the bonding molecular orbital. Two different geometries are possible which in turn give two types of bonds. The first one is when two electrons in a covalent bond are shared in a region of space common to the bonding atoms. This region of space is pictured as an overlap of two atomic orbitals. Such a bond that is cylindrically symmetrical around an axis joining the two nuclei is called sigma (σ) bond. The other bond is the pi (π) bond that is formed by sideways overlap of parallel p orbitals. Electrons in the π bond

are not concentrated along an axis between the two atoms but are shared in regions of space above and below the plane defined by the sp^2 orbitals.

Bonds in organic compounds are formed from hybrid orbitals that result from the mixing of two or more orbitals in the bonded atoms. This mixing process is called orbital hybridization. As a result of hybridization, two or more hybrid orbitals can be formed from atomic orbitals that are not identical. The number of hybrid atomic orbitals created is the same as the number of atomic orbitals used in hybridization.

Let us consider the bonding in methane, CH_4. The electronic configuration of carbon in the atomic state is $1s^2\ 2s^2\ 2p_x^1\ 2p_y^1\ 2p_z^0$. Methane has a tetrahedral structure, and all four C-H bonds are equivalent. The tetrahedral geometry of methane results from hybridization of the 2s and the three 2p orbitals of carbon which combine to form four equivalent hybrid orbitals, which are called sp^3 orbitals. The electronic configuration of this hybrid orbital is $1s^2\ 2s^1\ 2p_x^1\ 2p_y^1\ 2p_z^1$. Each hybrid atomic orbital overlaps with 1s orbital of hydrogen to form a σ bond.

The bonding electron in the double bond of ethylene, in which each carbon atom is bonded to three atoms, can be pictured with three sp^2 hybrid orbitals and one remains 2p orbital. The three sp^2 hybridized orbitals are used to make σ bonds. The second bond of the double bond in ethylene results from a side by side overlap of the p orbital of each carbon atom, which is a π bond. We note also

that there is another class of orbital hybridization for triple bond carbons such as acetylene, which is known as sp hybrid orbital [18].

The nature of orbital hybridization has a significant impact on the structures of polymers. Organic polymers having sp^3 hybridization are bound to form σ bonds only. Consequently the separation between valence band (bonding molecular orbital) and conduction band (anti-bonding molecular orbital) is large. Thus the localized states will have a large energy gap. Unlike sp^3 hybridization, sp^2 hybridization has π bonds in addition to the σ bonds, which yields smaller separation between the valence band and the conduction band and hence smaller energy gap. This class of polymers that have a combination of both σ- and π-bonds can be categorized into two forms, namely, those with localized and delocalized electronic states. The polymers with delocalized electronic configuration are capable of being doped to high electrical conductivity.

2.3 Peierls Transition

Polymers are quasi one-dimensional chains. Thus we need to understand the physics of one-dimensional metals first.

The regular arrangement of atoms or molecules in a crystal is caused by chemical bonding that keep the atoms in their position. Objects of equal mass connected to each other by elastic springs with different force constants or unequal masses connected with springs of the same force constant, may be taken as a model of one-dimensional crystals. Oscillation of the adjacent atoms will occur due to the strain in the spring that intern develops a wave. These waves are

sound waves, and the particles corresponding to the sound waves are called phonons.

Peierls distortion is an important case of electron-lattice coupling. To understand the basic principle of Peierls transition, we can consider a very idealized case of a one-dimensional linear chain, say, a linear equidistant arrangement of sodium atoms as shown in Fig. 2.2a. For such a chain the dispersion is parabolic on both sides as shown in Fig. 2.2b.

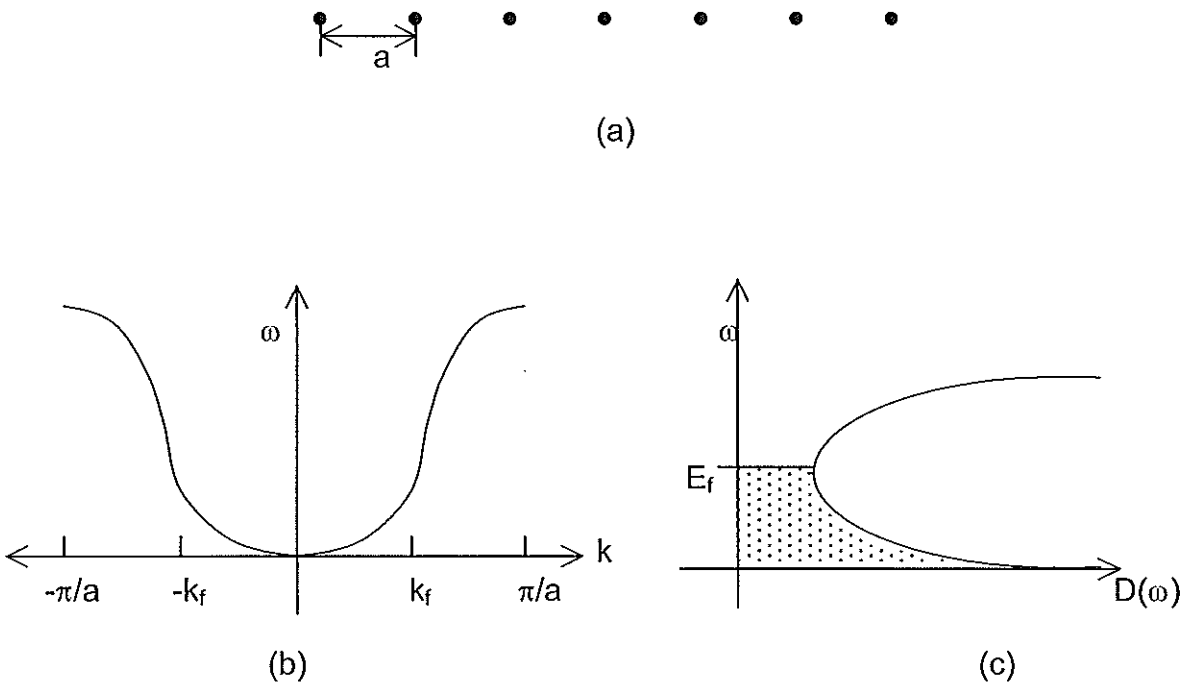

Fig. 2.2 (a) Undistorted crystal lattice in one dimension, (b) its dispersion relation and (c) its electronic density of states [2].

The density of states can be determined from [19]

$$D(\omega) = \frac{V}{(2\pi)^3} \int \frac{ds_\omega}{v_g} \qquad (2.1)$$

Where v_g is the group velocity and given by

$$v_g = \frac{1}{\hbar} \nabla_k \vec{E} \tag{2.2}$$

There is a singularity in density of states whenever the dispersion relation $\omega(k)$ is horizontal; i.e., whenever the group velocity is zero at $k = \pm \pi/a$.

Each sodium atom contributes one electron to the linear chain, whereas two electrons with opposite spins can be accommodated in each state. Hence the band is half-filled. The Fermi wave vector k_f is halfway between 0 and π/a and the Fermi energy E_F is at the band center.

Now suppose that the lattice is distorted in such a way that every second atom is displaced by an amount δ so that the atoms are no longer equidistant. In this case short distances $a - \delta$ and long distances $a + \delta$ alternate while keeping the arrangement still periodic, but with a repeating unit "2a" instead of "a" as shown in Fig. 2.3a.

The effect of such a distortion was first studied in 1955 by Peierls [20]. Peierls theorem states that a one-dimensional metal will be unstable against a metal to semiconductor transition and an energy gap will open up due to the occurrence of the lattice distortion so that the material becomes either insulator or semiconductor.

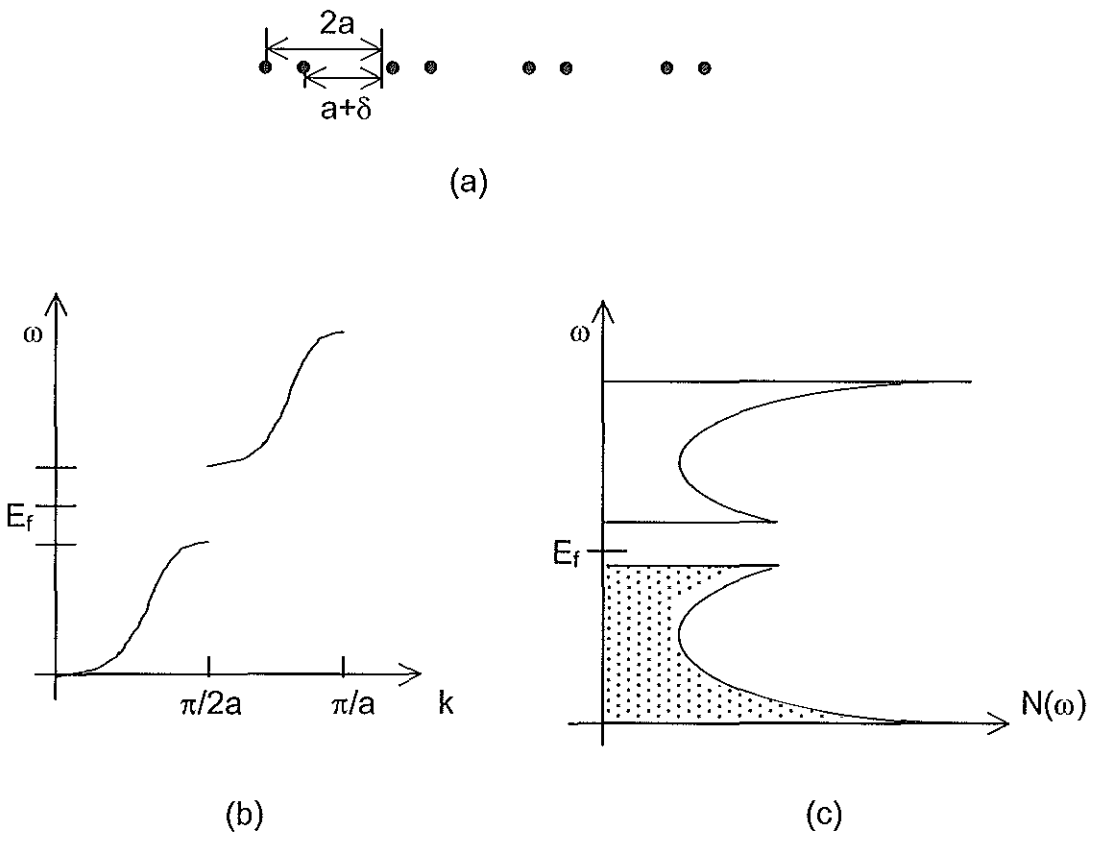

Fig. 2.3 Peierls distortion of a one-dimensional crystal [2]

(a) Crystal lattices (b) dispersion relation and (c) density of states.

As a consequence of the change in the repeating length, the boundary of the first Brillouin zone changes from $\frac{\pi}{a}$ to $\frac{\pi}{2a}$, see Fig. 2.3b. Therefore, unlike the former lattice, which caused the electrons to have a gap at $\frac{\pi}{a}$, the new lattice will create an additional gap at $\frac{\pi}{2a}$. Thus the distortion transforms the system from a metal with no gap at the Fermi level into a semiconductor or insulator with a gap. At absolute zero all states below the gap are filled and above the gap are empty. Such electron-lattice coupling will change the one-dimensional metal into a semiconductor (or insulator).

2.4 Peierls distortion in Polyacetylene

The existence of the alternating single and double bonds allow polyacetylene (PA) to have a number of possible structures as shown in Fig. 2.4.

(a)

(b)

Fig. 2.4 (a) Two phases of ground state degenerate dimerized *trans*-polyacetylene, (b) Two phases of ground state non-degenerate dimerized *cis*-polyacetylene.

Polyacetylene (PA) is said to be undimerized when all bond lengths along the PA backbone are equal and the spare electrons are delocalized over the whole system, see Fig. 2.5(a). It becomes dimerized when the electrons are localized to form alternating single and double bonds. The bond lengths are not equal, see Fig. 2.5(b). Undimerized PA is similar to undistorted chain of atoms with lattice constant "a" and dimerized PA is similar to distorted chain of atoms with lattice constant "2a". The dispersion relations for both types of PA are also shown in Fig. 2.5(c) and in Fig. 2.5(d).

In polyacetylene there is an alternation of single and double bonds. The double bonds are slightly shorter than the single bonds. This difference in bond

length distorts the regular array of the lattice and doubles the elementary cell of the one-dimensional crystal from lattice constant "a" to '2a". Doubling of the lattice constant in real space corresponds to reducing the first Brillouin zone by half in reciprocal space. This introduces a discontinuity in the dispersion relation, see Fig. 2.5d. Thus dimerization of the undimerized polyacetylene changes the PA from metallic state to non-metallic state.

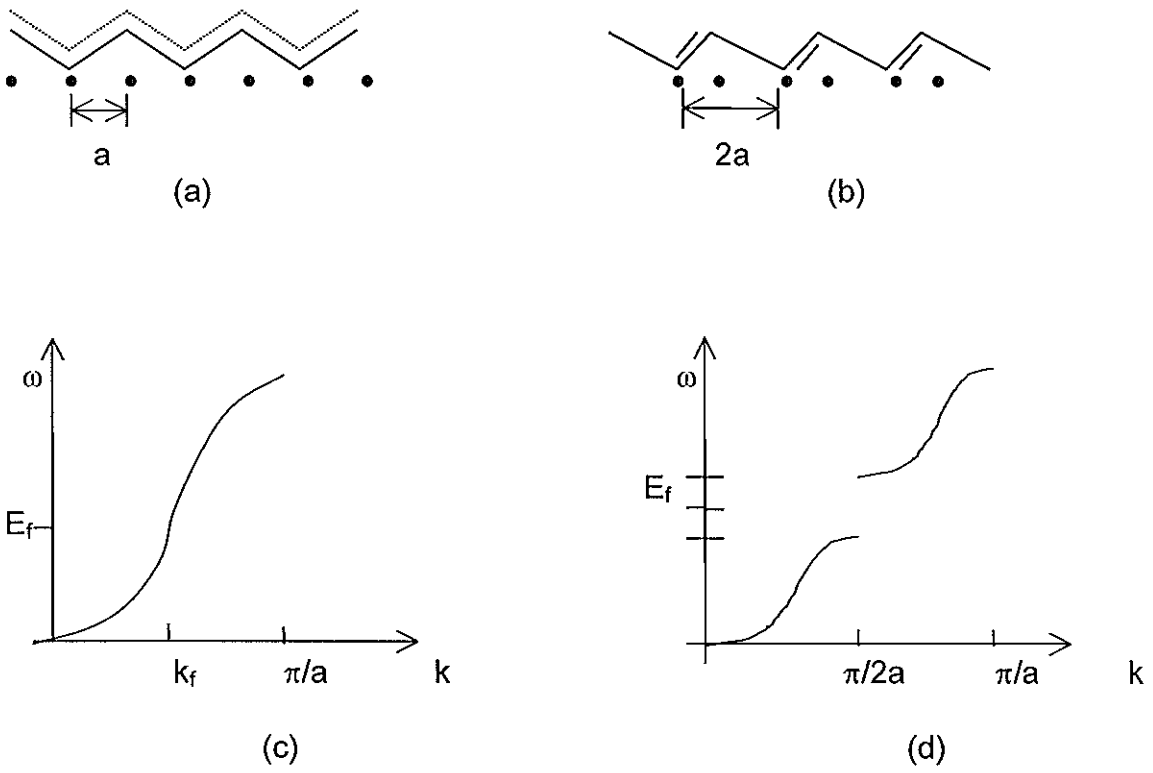

Fig. 2.5 Peierls distortion in polyacetylene. Undimerized PA (a) and its dispersion relation (c), Dimerized PA (b) and its dispersion relation (d).

2.5 Conjugational defects

In *trans*-conformation of polyacetylene there exist two energetically equal forms of degenerate ground states. The alternating single and double bonds can be oriented in two different directions. If the two phases of *trans*-conformations

are on the same chain as shown in Fig. 2.6, they will certainly be separated by a defect (misfit) in the bond alternation. Such a misfit is known as 'solitons' [21]. Since the two phases are energetically equal, this is a stable defect and may also be mobile.

Fig. 2.6 A misfit (soliton) separating the two phases of a *trans*-polyacetylene.

2.5.1 Solitons

The cause of energy gap formation is the uninterrupted double bond and single bond alternation. However, at the misfit (soliton site) the bond alternation is interrupted. At the misfits the atomic orbital is neither bonding nor anti-bonding; rather it forms a non-bonding state that lies in the middle of the energy gap [22].

There are neutral as well as positively or negatively charged solitons. Fig. 2.7 shows the valence (π) and the conduction (π^*) bands, and the soliton mid-gap state may be empty or can be occupied by up to two electrons. The ionic charge is compensated only when there is one electron at the defect site. If there is no electron the ion is left uncompensated and the soliton is positively charged; two electrons over compensate the ion and the soliton becomes negatively charged. Charged solitons are spinless, while neutral solitons carry a magnetic moment [23].

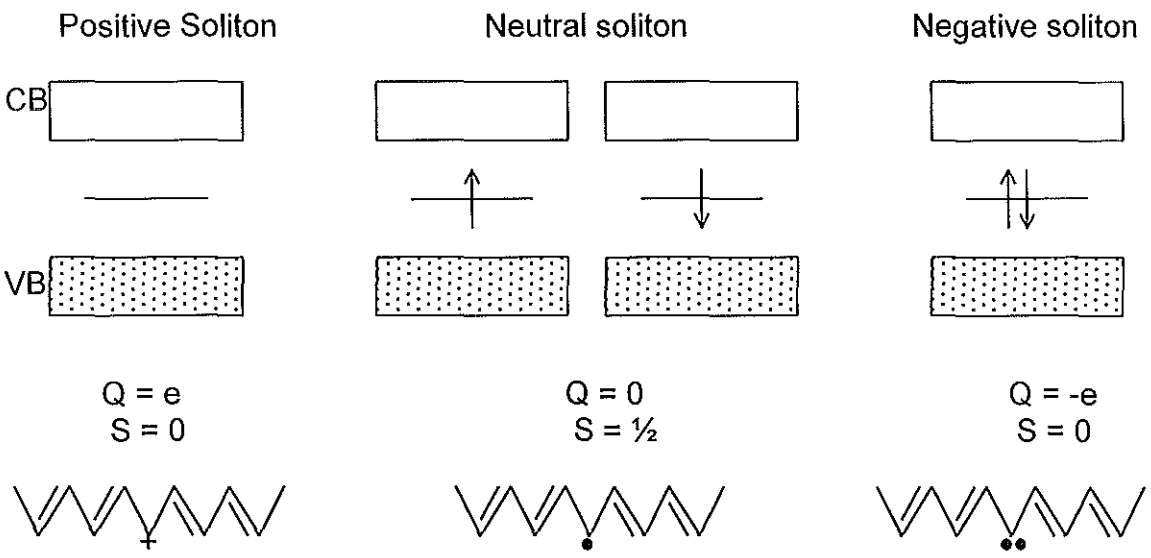

Fig. 2.7 Spin charge inversion of conjugated polymer.

2.5.2 Polarons and Bipolarons

Polaron is used to represent a localized electron state and the associated lattice distortion. It is described as a bound state of a soliton and anti-soliton. Polyacetylene has both degenerate and non-degenerate ground states. However, many other conjugated polymers have non-degenerate ground states. Figure 2.8 shows the two forms of non-degenerate polythiophene.

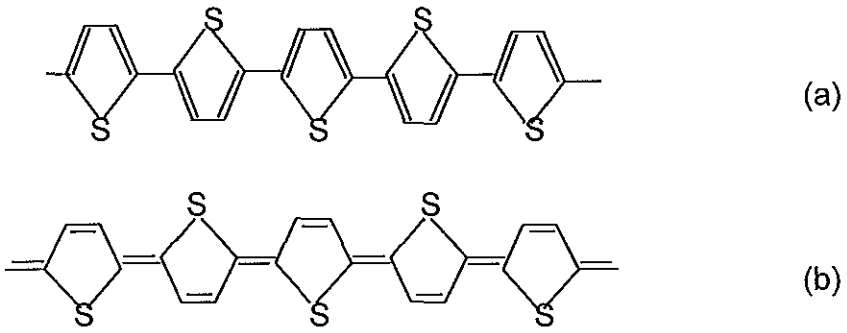

Fig. 2.8 Two non-degenerate forms of polythiophene

(a) aromatic form and (b) quinoidal form.

The aromatic form is the lowest energy state and the quinoidal form is the highest energy state. In polythiophene the soliton separates the aromatic (low energy) region from a quinoidal (high energy) region. The soliton will be driven to the chain end, changing the high-energy quinoidal rings into low energy aromatic rings as it moves as depicted in Fig. 2.9.. Therefore, solitons in non-degenerate polymers are energetically unstable.

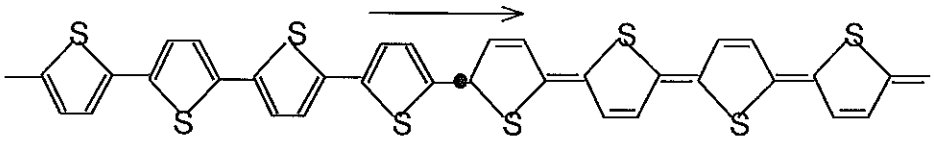

Fig. 2.9 Motion of a Soliton in polythiophene.

If defects in non-degenerate ground state polymers are to be stable, bound double defects must be created. Singly charged states are called polarons and doubly charged states are called bipolarons. These states are shown in Fig. 2.10(a) and Fig. 2.10(b), respectively.

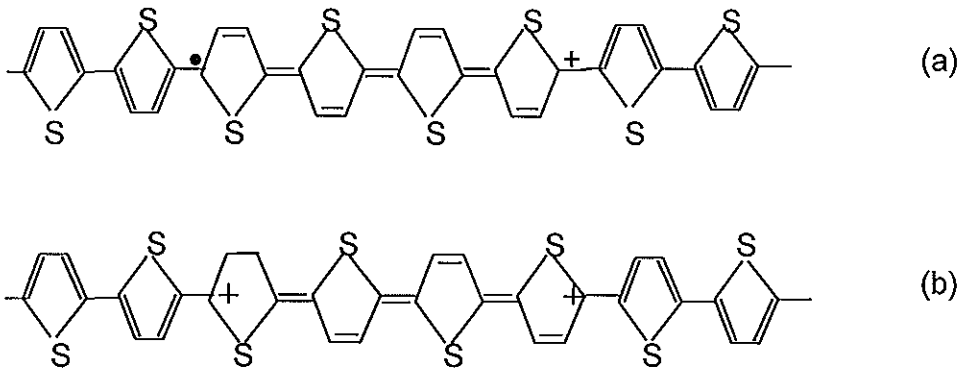

Fig. 2.10 Formation of a polaron (a) and a bipolaron (b) in polythiophene.

A polaron is characterized by two states in the gap. The emergence of two states can be rationalized to occur through interaction between the midgap states belonging to the soliton components of the polaron. New electronic states are created in the energy gap when oxidizing a non-degenerate ground state polymer. The schematics of the energy band diagram for both polaron and bipolaron are shown in Fig. 2.11.

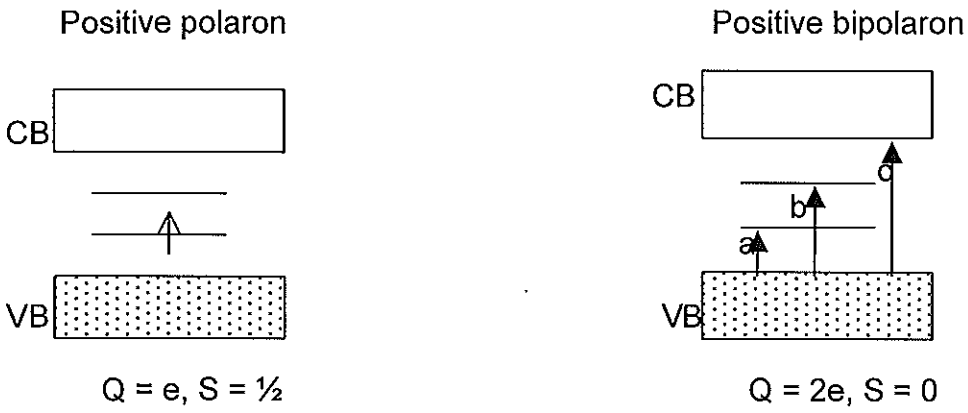

Fig. 2.11 Energy band diagrams of positive polaron and positive bipolaron and possible transitions of charge carriers.

The existence of polaron and bipolaron states is experimentally confirmed using optical absorption spectrum of PTOPT, Fig. 2.12 [24]. As depicted in Fig. 2.11, 'a' refers to transition from valence band to the lower state, 'b' represents transition from valence band to the upper state, and 'c' refers to the interband transition.

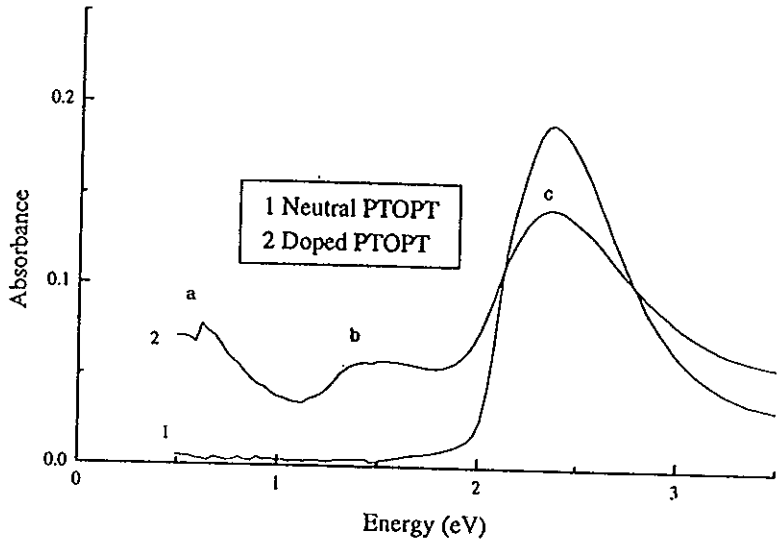

Fig. 6.12 Absorption spectrum of PTOPT

2.6 Charge transport mechanism

The conduction mechanism of electrically conducting polymer has been widely investigated with polyhetrocycles such as polypyrolle [25], polyacetylene [26] and poly(3-hexylthiophene) [27]. In actual conjugated polymers carriers do not only hop along the chain but also hop across the interchain and interfibrill gaps. In this respect temperature dependence of electrical conductivity is important.

In pure undoped state, conjugated polymers have a very low electrical conductivity, which can be explained by small thermal excitation of charge carriers over the band gap. However, the conductivity can increase drastically by doping.

Due to the complex structural and morphological forms of conducting polymers a single model can not explain the charge transport process over the whole conductivity range from insulators to metals. Thus for these various

conductivity ranges different models are needed. Charge transport mechanism of undoped or lightly doped conjugated polymers can be explained by hopping (phonon-assisted quantum mechanical tunneling) mechanism between the localized solitonic, polaronic or bipolaronic states [28]. These states are localized in the gap and are randomly distributed in space as well as in energy. The states below E_f are occupied and those above are empty except in case of thermal excitation. Electrons will hop from occupied to empty states.

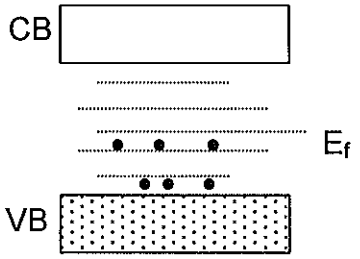

Fig. 2.12 Random distribution of different states in the gap.

There are many phonons available at high temperatures that can assist the hopping. As these phonons freeze due to cooling, the electron has to look for an energetically accessible state. Consequently, the average hopping distance will decrease as the temperature decreases, hence the name "variable range hopping". The tunneling probability decreases exponentially with distance, which results in exponential decrement in the conductivity.

The temperature dependence of conductivity can be described by [2]

$$\sigma = \sigma_0 \exp\left[-\left(\frac{T_o}{T}\right)^{\gamma}\right] \tag{2.3}$$

where γ depends on the dimensionality d of the hopping process and is given by

$$\gamma = \frac{1}{1+d} \tag{2.4}$$

For three-dimensional variable range hopping, γ = ¼ and eq. (2.3) gives Mott's famous $T^{-\frac{1}{4}}$ law at low temperature [29].

$$\sigma = \sigma_0 \exp\left[-\left(\frac{T_o}{T}\right)^{\frac{1}{4}}\right] \tag{2.5}$$

where $$\sigma_o = e^2 N(E_f) R \nu_{ph} \tag{2.6}$$

$$R = \left[\frac{8}{9}\pi\alpha N(E_f) kT\right]^{-\gamma} \tag{2.7}$$

and $$T_o = \frac{8^3 \alpha^3}{9\pi k N(E_f)} \tag{2.8}$$

R is the average hopping distance, $N(E_f)$ is electronic density of states at the Fermi energy, α is inverse localization length (spatial extension of localized wave function), ν_{ph} is typical phonon frequency. The model has been shown to be appropriate for poly(3-hexylthiophene) [27], polyacetylene [30], and polypyrrole [31].

For highly doped conducting polymers other models have been shown to be useful. The model of variable range hopping assumes a random distribution of localized states. If the distribution is not random and the defects tend to cluster, the model of "fluctuation induced tunneling" is more appropriate [32, 33]. This model assumes that conduction takes place between highly conductive islands

separated by potential barriers. The origins of these islands are believed to be from conjugational defect, inhomogeneous aggregations of dopant molecules, segments of undoped or weakly doped polymer chain, interchain or inter-fibrillar contacts.

In this model tunneling enhanced by thermal fluctuations at higher temperature through these barriers is responsible for charge transfer. The model gives the temperature dependence of the conductivity as

$$\sigma(T) = \sigma_o \exp\left(-\frac{T_1}{T_o + T}\right) \tag{2.9}$$

where the constants σ_o, T_o, and T_1 are determined by the geometry of the barrier and the size of the conducting islands.

3 Electrical properties of metal-polymer contacts

Conjugated polymers have been extensively studied for their applications in electronic and optoelectronic devices such as light emitting diodes (LED) [6-11], field-effect transistor (FET) [12,13] and other surface junction devices. In all these applications the nature of the metallic contact to the polymer plays an important role.

3.1 Metal-semiconductor contact

The work function of a metal (ϕ_m) is the amount of energy required to raise an electron from the Fermi level to a state of rest outside the surface of the metal that is called vacuum level. The work function (ϕ_s) of a semiconductor is the difference in energy between the Fermi level and the vacuum level [34].

When a metal makes an intimate contact with a semiconductor, a Schottky barrier may be formed at the junction. To see how a Schottky barrier may form at the contact, consider electrically neutral metal and semiconductor, which initially are separated from each other. Fig. (3.1a) and Fig. (3.1b) show the energy band diagrams of the metal with work function greater than that of an n-type semiconductor ($\phi_m > \phi_s$) before they have been brought in to contact and after contact, respectively.

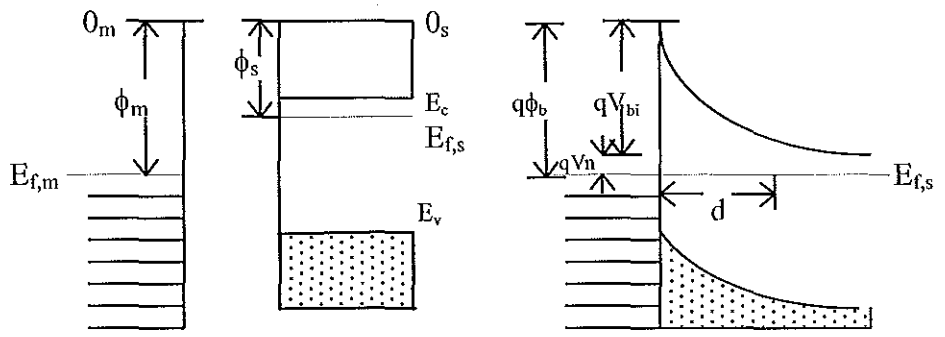

(a) (b)

Fig. 3.1 Energy band diagram of metal-n-type semiconductor before (a) and after (b) contact for $\phi_m > \phi_s$.

After the contact is made, electrons will flow out of the semiconductor into the metal until the Fermi energies, $E_{f,m}$ of the metal and $E_{f,s}$ of the semiconductor, coincide and a state of equilibrium is achieved [35]. A built-in potential (V_{bi}) will be established between the metal and the semiconductor. As a result, a positive space charge throughout the barrier width "d" is built up. The difference between the bottom of the conduction band, E_c, and the Fermi energy, E_f, in the bulk of the semiconductor is qV_n, and ϕ_b is the barrier height. Therefore, as the electron moves inside the space charge layer, its potential energy $\varphi(x)$ increases and reaches its maximum value $\varphi_o = qV_{bi}$ at the semiconductor-metal interface.

By using Poisson's equation, $\varphi(x)$ can be derived and is given by [36]

$$\varphi(x) = [(q^2N_d)/(2\varepsilon_o\varepsilon)](d - x)^2 \qquad (3.1)$$

where N_d is donor concentration.

If the work function of the metal is less than that of an n-type semiconductor, the electrons shall be transported from the metal to the semiconductor setting up a negative charge in its contact layer. In this case the energy of the electron $\varphi(x)$ decreases as it approaches the surface. This leads to an increase in the free charge carrier concentration inside the contact layer of the semiconductor and increases its conductivity. For this reason such a layer is ohmic (see Fig. 3.2) [36].

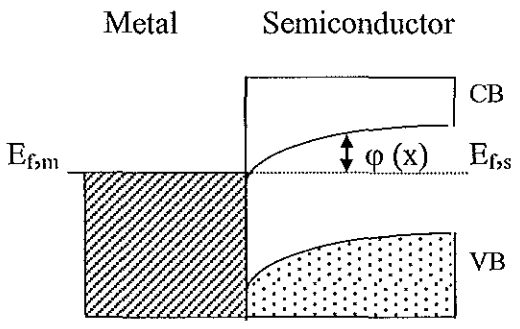

Fig. 3.2 Band diagrams for n-type semiconductor-metal contact with $\phi_m < \phi_s$.

In the case of a p-type semiconductor, if $\phi_m > \phi_S$, we obtain the band diagram shown in Fig. (3.3a) which represents ohmic contact. However, $\phi_m < \phi_S$ gives rise to rectification, Fig. (3.3b).

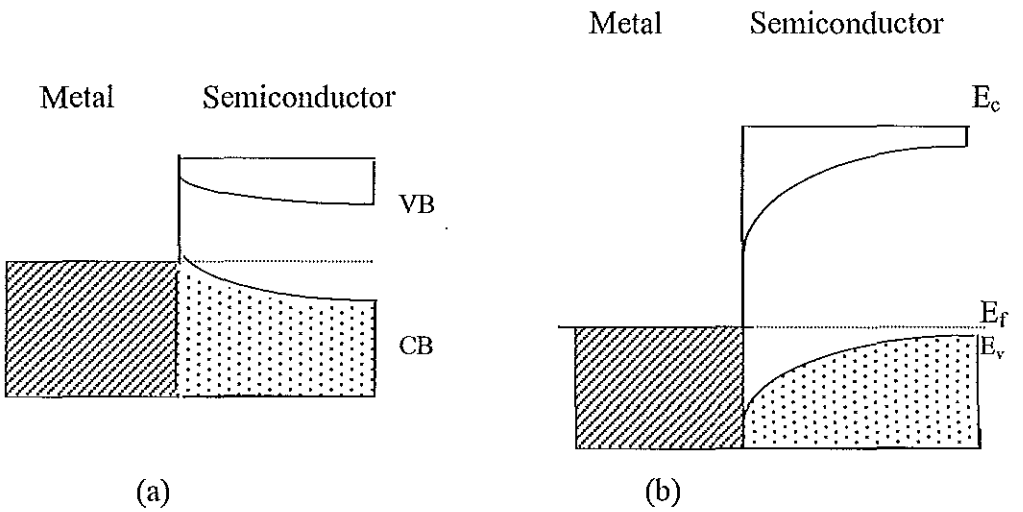

Fig. 3.3 Band diagrams for p-type semiconductor-metal contact for (a) $\phi_m > \phi_s$, which is ohmic and (b) $\phi_m < \phi_s$, which is a rectifying contact.

These are the phenomena that are observed for a p-type semiconducting polymer-metal interface.

3.2 Current-voltage characteristics

There are various ways in which electrons and holes can be transported across a metal-semiconductor junction under forward bias. These are: (a) emission of electrons from the semiconductor over the top of the barrier into the metal (the dominant process for Schottky diodes with moderately doped semiconductors), (b) quantum mechanical tunneling through the barrier (important for heavily doped semiconductors and responsible for most ohmic contacts), (c) recombination in space charge region, and (d) recombination in the neutral region, (see Fig. 3.4.) [34].

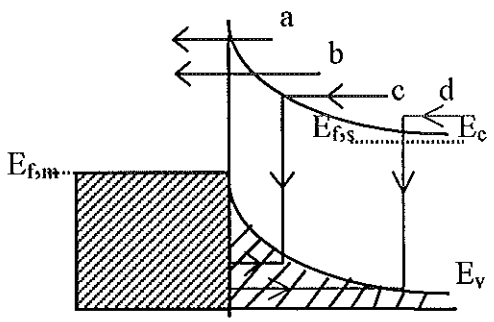

Fig. 3.4 Four basic transport processes under forward bias Schottky barrier diode.

The transport equation of an ideal metal-semiconductor rectifying contact is given by a Schottky barrier diode equation

$$J = J_s[\exp\left(\frac{qV}{nkT}\right) - 1] \tag{3.2}$$

where

$$J_s = A^{**}T^2 \exp\left(-\frac{q\phi_b}{kT}\right) \tag{3.3}$$

where J is the total current density, J_s is the reverse saturation current density, q is the charge of an electron, V is the applied forward bias voltage, k is Boltzmann's constant, T is absolute temperature, n is diode ideality factor, ϕ_b is barrier height and A^{**} is modified Richardson constant which expresses the number of electrons at the semiconductor-metal interface that may be injected into the metal. A^{**} also takes into account the effective density of states in the conduction band. For organic semiconductor Schottky diodes the modified Richardson constant is assumed to be that of a free electron, namely, A^{**} = 120 $A/cm^2 K^2$ [37, 38].

The Schottky diode eq. (3.2) can be studied under three different conditions:

(1) If $J >> J_s$, the contact will effectively block current flow for a reverse bias voltage and will display an exponentially increasing current for a forward bias. This results in a rectifying contact.

(2) If $J << J_s$, the junction readily passes current for both signs of the applied voltage. In this case eq. (3.2) can be expanded to yield

$$V \cong \left(\frac{n\,k\,T}{J_o\,q} \right) J \tag{3.4}$$

This equation is linear in J and is Ohm's law.

(3) If $J \cong J_s$, i.e., if J and J_s are comparable, then the J-V curve is neither rectifying nor ohmic but symmetric.

J_s can be obtained experimentally by extrapolating linear part of the logJ versus V plot to the logJ axis at a small forward bias. The intersection of this line with logJ axis gives J_s. Once J_s is obtained, it is possible to calculate the barrier height ϕ_b and the ideality factor "n" from eqs. (3.2) and (3.3).

3.3 Capacitance-voltage measurements

The space charge Q_{sc} of the semiconductor and the depletion layer capacitance are given by

$$Q_{sc} = qN_D dA \tag{3.5}$$

$$Q_{sc} = A\sqrt{2q\varepsilon_s\varepsilon_o N_D(V_{bi} - V - kT/q)} \tag{3.6}$$

$$C = \left|\frac{\partial Q_{sc}}{\partial V}\right| = A\sqrt{\frac{q\varepsilon_s\varepsilon_o N_D}{2(V_{bi} - V - kT/q)}} = \frac{\varepsilon_s\varepsilon_o A}{d} \tag{3.7}$$

where A is the cross sectional area of the device, ε_s is the dielectric constant of the polymer, ε_o is permitivity of free space, N_D is the dopant density and V is the applied voltage.

Equation (3.7) can be rewritten as

$$\frac{1}{C^2} = \frac{2}{qA_s^2\varepsilon_o\varepsilon_s N_D}(V_{bi} - V - kT/q) \tag{3.8}$$

or

$$-\frac{d(1/C^2)}{dV} = \frac{2}{q\varepsilon_s\varepsilon_o N_D A_s^2} \tag{3.9}$$

Thus,

$$N_D = -\frac{2}{q\varepsilon_o\varepsilon_s A_s^2}\frac{1}{d(1/C^2)/dV} \tag{3.10}$$

If N_D is constant throughout the depletion region, one should obtain a straight line by plotting $1/C^2$ versus reverse bias Voltage. If N_D is not constant, the differential capacitance method can be used to determine the doping profile from eq. (3.10), [35].

The above formulation is limited to an ideal metal-semiconductor contact with no interfacial layers of any kind separating them. However, the case of metal-insulator-semiconductor is of a paramount importance in device physics. The depletion width can also be obtained from C-V measurement. Combining eqs. (3.7) and (3.8) yields

$$\frac{d^2}{\varepsilon_s^2 \varepsilon_o^2 A^2} = \frac{2}{qA_s^2 \varepsilon_o \varepsilon_s N_D}(V_{bi} - V - kT/q) \tag{3.11}$$

Thus

$$d = \left[\frac{2\varepsilon_o \varepsilon_s}{qN_D}(V_{bi} - V - kT/q) \right]^{1/2} \tag{3.12}$$

3.4 Impedance Spectroscopy

Impedance spectroscopy is a relatively new and powerful technique for characterizing materials and their interfaces with their electronically conducting electrodes. The common approach to measure impedance is by applying voltage to the electrode interface and measuring the amplitude and the phase shift of the resulting current in the frequency domain. Impedance spectroscopy has been used to study electrical and dielectric properties of polymers [24, 39-42], progress of reactions in polymer forming systems [43].

The applicability of impedance spectroscopy method to the studies that give direct correlation between the response of a real system and an idealized model circuit composed of discrete electrical components makes it more attractive. The very important idea in the modeling studies is to match experimental impedance results with the impedance of ideal resistor and capacitor equivalent circuit [44].

The circuit model contains only a resistor and a capacitor, which describes the dissipative components of the dielectric response and the storage component of the dielectric material. Inductance, which requires the storage of energy in a

magnetic field, is not included in the circuit model because there is no appreciable alternating current magnetic field energy in the low current impedance spectroscopy measurements.

A very simple modeling concept can be seen by considering a parallel circuit made of a resistor and a capacitor as shown in Fig. (3.5).

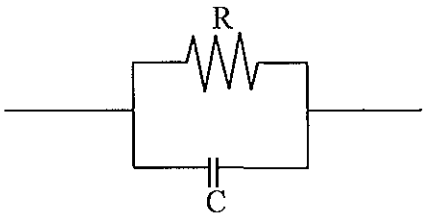

Fig. 3.5 Paralle RC circuit.

The impedance for the above RC circuit is given by

$$Z = \frac{R}{1 + j\omega RC} = \frac{R}{1 + \omega^2 R^2 C^2} - j\frac{R^2 \omega C}{1 + \omega^2 C^2 R^2} \tag{3.13}$$

where j is the imaginary number defined by $\sqrt{-1}$ and ω is the frequency. Thus from eq. (3.13) real and imaginary parts are separated as:

$$\mathrm{Re}(Z) = \frac{R}{1 + \omega^2 R^2 C^2} \tag{3.14}$$

and

$$-\mathrm{Im}(Z) = \frac{R^2 \omega C}{1 + \omega^2 R^2 C^2} \tag{3.15}$$

The Cole-Cole [45] plot of this circuit, in its ideal form, will be a semi-circle whose center lies on the Re(Z) axis, Fig. 3.6.

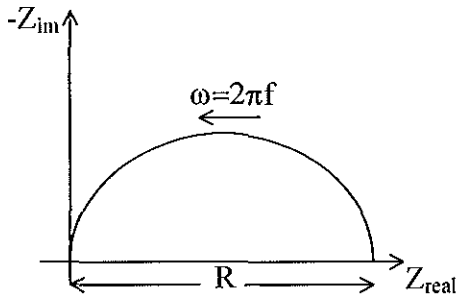

Fig. 3.6 Cole-Cole plot of parallel RC circuit.

If there is a contact resistance R_c in series with the RC parallel circuit shown in Fig. (3.5), the impedance given by eq. (3.14) becomes

$$Z = R_c + \frac{R}{1 + j\omega RC} \tag{3.16}$$

whose Cole-Cole plot is depicted in Fig. 3.7(b).

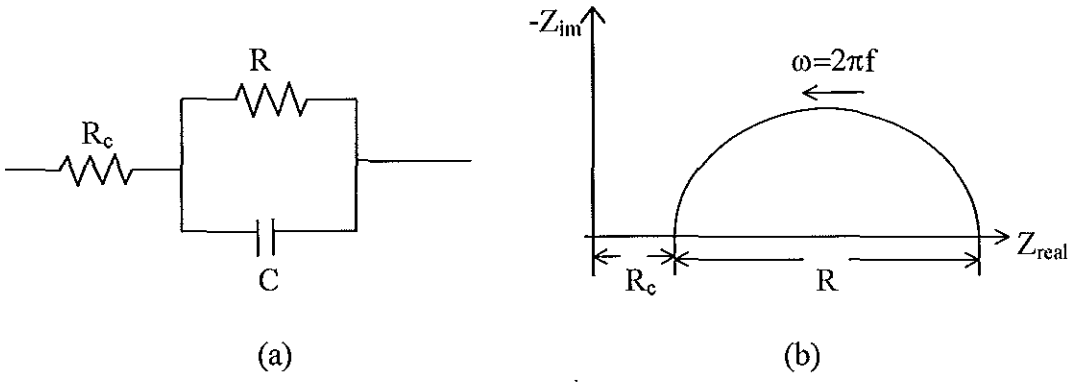

Fig. 3.7 Circuit for a contact resistance R_c connected in series with parallel RC circuit (a) and its Cole-Cole plot (b).

The circuit model represented by Fig. (3.7) is an equivalent circuit model for a metal-semiconductor junction in which the depletion region accounts for the observed capacitance and resistance and the contact resistance accounts for the resistance of connecting wires.

Another model, which is equivalent to a metal-insulator-semiconductor device, can be obtained by considering two parallel RC circuits in series with R_c as shown in Fig. (3.8).

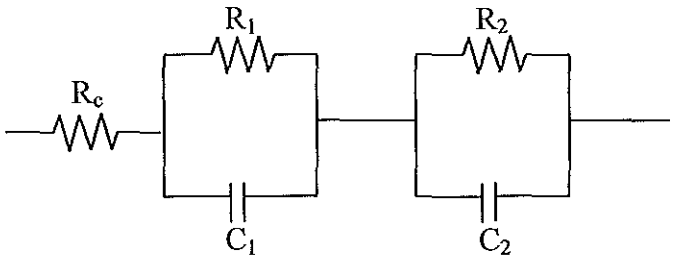

Fig. 3.8 An equivalent RC circuit of metal-insulator-semiconductor device.

The complex impedance of the circuit in Fig. (3.8) is given by

$$Z = R_c + \frac{R_1}{1 + j\omega R_1 C_1} + \frac{R_2}{1 + j\omega R_2 C_2} \tag{3.17}$$

Here, R_1 and C_1 represent the interfacial insulating thin layer and R_2 and C_2 account for the depletion region. The Cole-Cole plot for such a model is shown in Fig. (3.9).

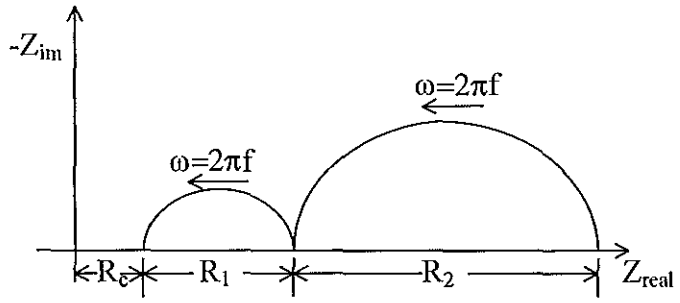

Fig. 3.9 Idealized Cole-Cole plot for the circuit shown in Fig. (3.8).

Many reports [24, 39-41] reveal the existence of an insulating interfacial layer between conjugated polymers doped with large anions and reactive metals, yielding two partially overlapping semicircles in a Cole-Cole plot. The depletion region resistance and capacitance are voltage-dependent.

4. Thickness Dependence of Optical Electric Field of Polymeric Diodes

In this thesis a single layer diode i.e., Al/PEOPT/ ITO, is studied. However, a theoretical aspect of the effect of increasing the number of layers in the device will be presented for future use. As the number of layers in the device is increased, light reflection at the interface due to the difference in the complex index of refraction ($n = n'-ik$) of each material included in the multi-layer devices has to be considered.

The square of the normalized electric field $|E|^2$ at the interface can be derived to see the effect of thickness and index of refraction of the materials in the multi-layer device.

The classical model of a damped harmonic oscillator can describe the excited atomic electron of charge q, frequency ω, mass m and restoring force constant k_o under the influence of a driving force qE caused by the incident wave with amplitude $E = E_o e^{i\omega t}$ [46]. The corresponding differential equation becomes

$$m\ddot{x} + m\gamma\dot{x} + k_o x = qE_o e^{i\omega t} \tag{4.1}$$

The non-homogeneous solution for the differential equation (4.1) is

$$x = \frac{qE_o e^{i\omega t}}{m\left(\omega_o^2 - \omega^2 + i\gamma\omega\right)} \tag{4.2}$$

where $\omega_o^2 = \frac{k_o}{m}$.

The forced oscillation of the charge q generates an induced dipole moment p, which is given by

$$P = qx = \frac{qE_o e^{i\omega t}}{m\left(\omega_o^2 - \omega^2 + i\gamma\omega\right)} \tag{4.3}$$

In a sample with N oscillators per unit volume, the microscopic polarization P is given by

$$P = Nqx \tag{4.4}$$

For isotropic materials, the relationship between E and P becomes

$$P = \varepsilon_o \chi E \tag{4.5}$$

where ε_o is permitivity of free space and χ is the linear dielectric susceptibility.

The relative dielectric constant ε is related to the refractive index, n, by

$$n = \sqrt{\varepsilon} \tag{4.6}$$

Combining equations (4.1) to (4.6), the refractive index can be written as

$$n^2 = 1 + \frac{Nq^2}{\varepsilon_o m\left(\omega_o^2 - \omega^2 + i\gamma\omega\right)} \tag{4.7}$$

By applying binomial theorem equation (4.7) can be approximated as

$$n = 1 + \frac{Nq^2}{2\varepsilon_o m\left(\omega_o^2 - \omega^2 + i\gamma\omega\right)} \tag{4.8}$$

The physical implication of the complex index of refraction becomes clear if the real and imaginary parts of the refractive index are separated as

$$n = n' - ik \tag{4.9}$$

An electromagnetic wave $E = E_o e^{i(\omega t - kZ)}$ passing in Z-direction through a medium with the refractive index 'n' has the same frequency $\omega_n = \omega_o$ as in vacuum but a different wave vector $k_n = k_o n$. Thus

$$k_n = k_o(n' - ik) \tag{4.10}$$

Therefore, the electromagnetic wave becomes

$$E = E_o e^{i(\omega t - k_o n' Z + i k_o k Z)} \tag{4.11}$$

or $$E = E_o e^{-k_o k Z} e^{i(\omega t - k_o n' Z)} \tag{4.12}$$

The real part of this equation is

$$E = E_0 e^{-k_o k Z} \cos k_o(ct - n' Z) \tag{4.13}$$

The normalized electric field then becomes

$$|E|^2 = E_o^2 e^{-2k_o k Z} \cos^2 k_o(ct - n' Z) \tag{4.14}$$

Thus $|E|^2$ shows a damping periodic variation with thickness.

Fig. (4) shows the effect of variation of the index of refraction of the material on the optical electric field. In plotting Fig. 4, E_o, k_o, and ct were taken to be constant values.

Therefore, by choosing proper materials as electrodes and appropriately choosing the thickness of all the layers, one can optimize the optical field at the active interface and enhance the photogenerated current [47].

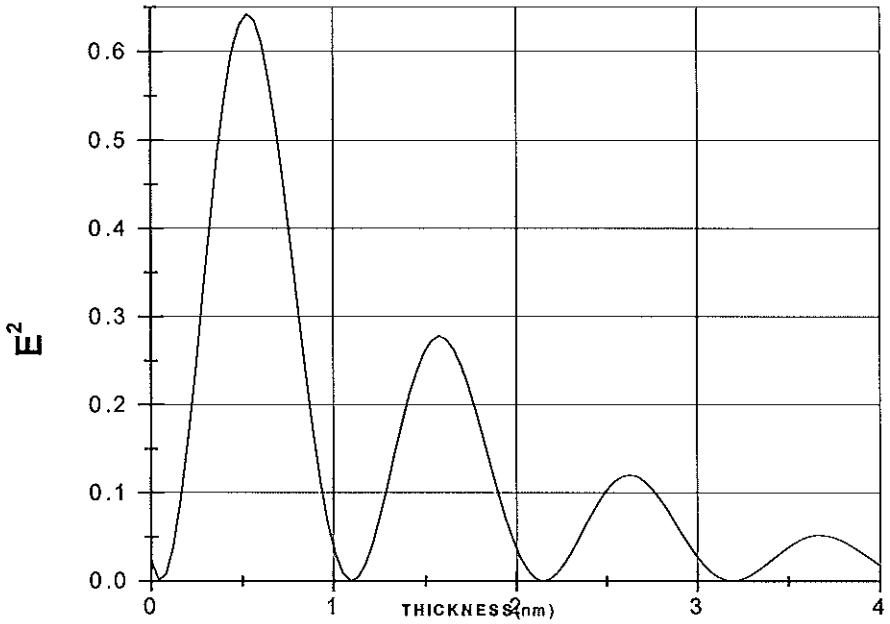
0.6
0.5
0.4
0.3
0.2
0.1
0.0
E2
0
1
2
3
4
THICKNESS(nm)

(a)

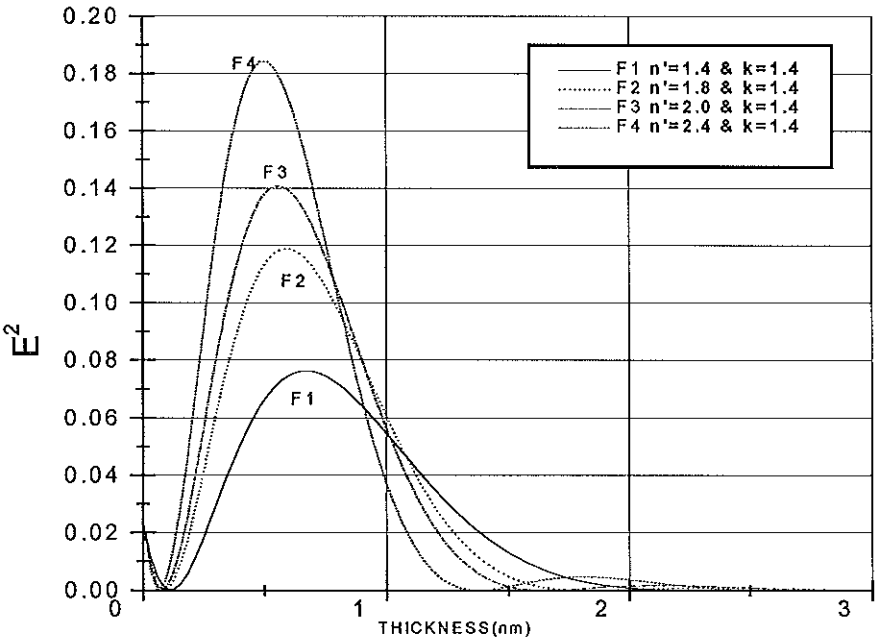
0.20
0.18
0.16
0.14
0.12
0.10
0.08
0.06
0.04
0.02
0.00
E2
F4
F3
F2
F1
F1 n'=1.4 & k=1.4
F2 n'=1.8 & k=1.4
F3 n'=2.0 & k=1.4
F4 n'=2.4 & k=1.4
0
1
2
3
THICKNESS(nm)

(b)

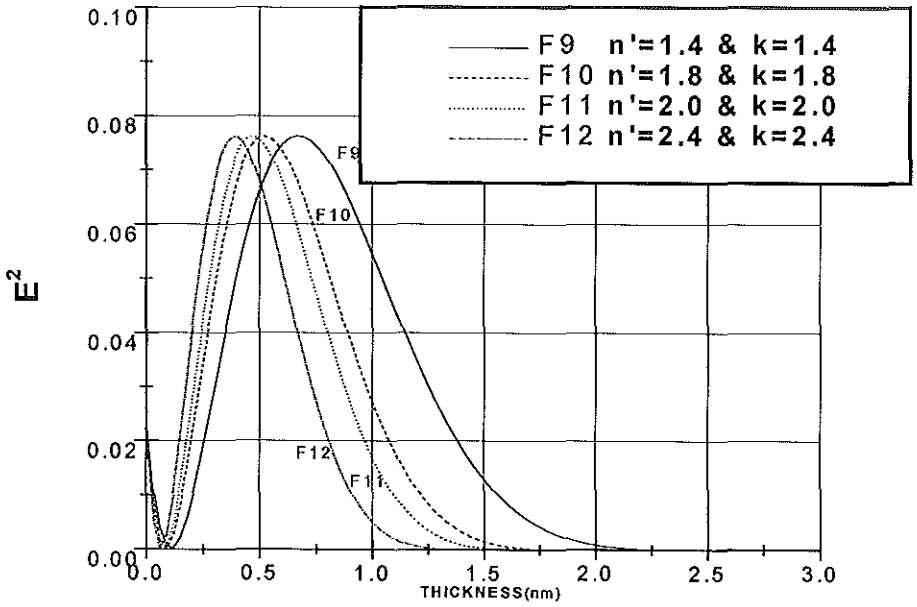

(c)

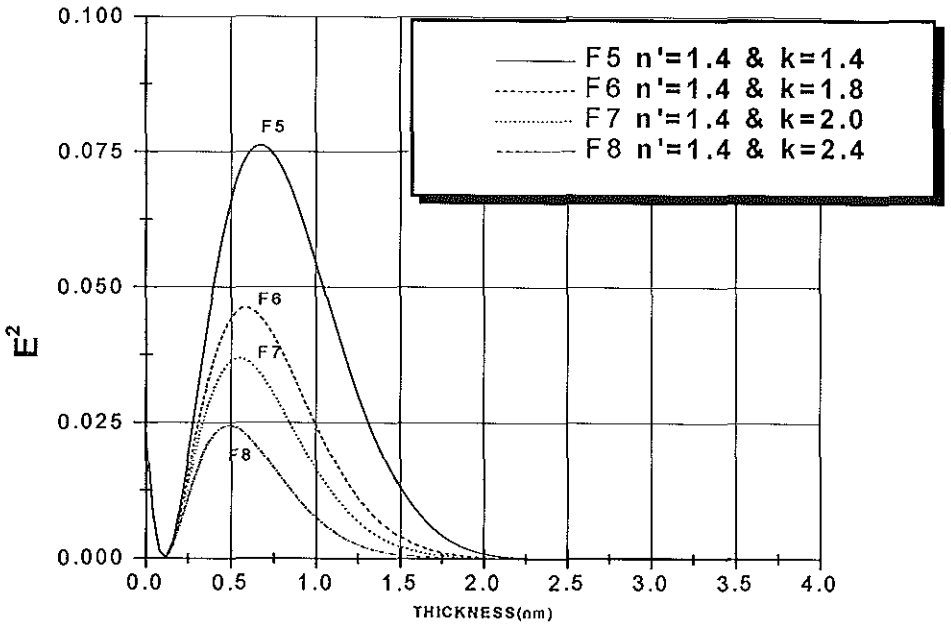

(d)

Fig. 4.1 (a) The variation of optical electric field as a function of thickness
(b), (c), and (d) show the effect of index of refraction on the optical electric field.

5. Experiment

5.1 Absorption Spectrum Measurement

An 8mg solid form of PEOPT was dissolved in 2ml chloroform to give a solution of PEOPT with a concentration of 4mg/ml, which was used for absorption spectra, current-voltage, and impedance spectroscopy measurements.

For optical absorption measurement, thin films of PEOPT were spin coated on clean glass substrates at a rate of 6000rpm yielding a uniform, high quality reddish-yellow solid films of about 200-300nm thickness. The thin film of PEOPT-on-glass prepared was then placed in the sample holder of Perkin Elmer λ19 UV/Vis/NIR spectrophotometer. With the help of ultra-violet computer spectroscopy software, UVCSS, interfaced to the computer, the absorption spectrum was obtained (see Fig. 6.1) and analyzed.

5.2 Current-voltage measurement

For electrical characterization, samples of Al/ PEOPT/ ITO two terminal devices were prepared as follows. Pre fabricated indium tin oxide (ITO) on glass was cut out in such a way that each piece has an area of about $9cm^2$ (see Fig.5.1a). These pieces were partly covered (about two-third) with photoresist, and the exposed part of ITO was etched with a mixture of concentrated hydrochloric acid, sulphric acid and water with 48:4:48 ratio by volume, respectively. Here the photoresist is to protect the covered part of the ITO from being etched. The etched part of the ITO/glass provideds a convenient region for

electrical contacts to the aluminum layer deposited later. The photoresist was then removed using acetone and the whole surface was washed with distilled water and methanol, and rinsed with ethanol (see Fig. 5.1b).

The PEOPT chloroform solution of concentration 4mg/ml was spin coated on the ITO/ glass substrate thus prepared at a speed of 6000rpm (see Fig. 5.1c). At this stage the polymer covers the whole area. For electrical contacts, part of the PEOPT from the etched part (pure glass) and the ITO part were cleaned with chloroform to obtain the structure shown in Fig. 5.1d that is ready for the deposition of aluminum.

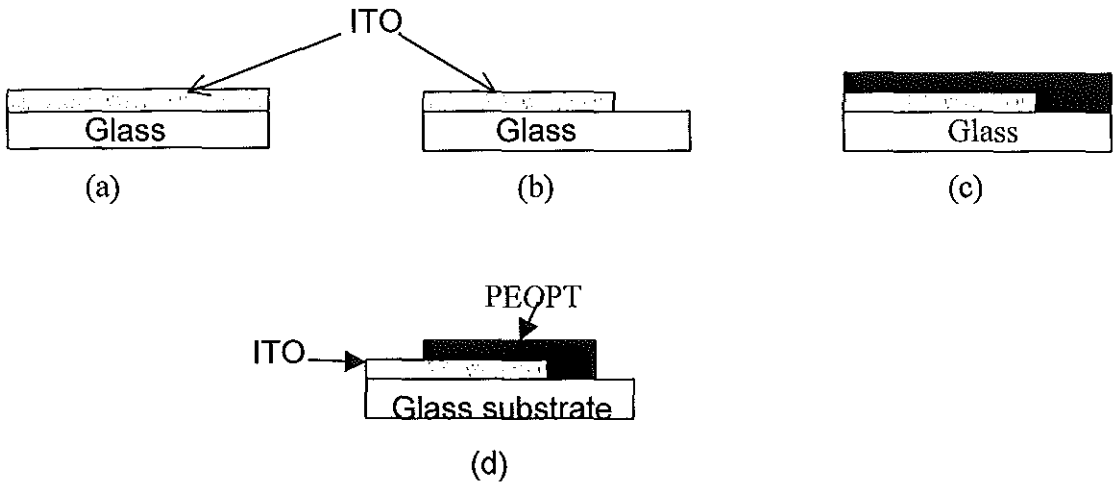

Fig. 5.1 Preliminary steps in preparing the device

Using Edwards Auto 306 vacuum evaporator, a low work function metal, aluminum, was evaporated at a pressure of about 7 x 10^{-6} mbar on the PEOPT-ITO-glass substrate to get the working sample Al/ PEOPT/ ITO-glass sandwich structure shown in Fig. 5.2.

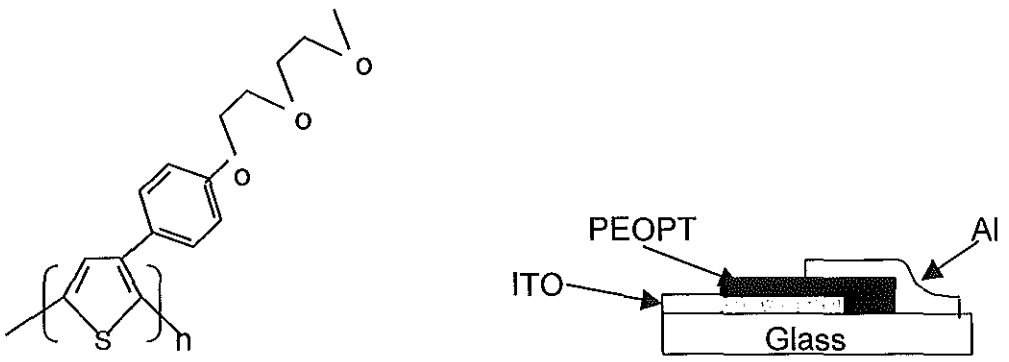

Fig. 5.2 Chemical structure of PEOPT and the sandwich Al/PEOPT/ITO-glass photodiode.

The area of the active junction of the device was about 5mm^2. The sandwich structure shown in Fig. 5.2 provides a means for current-voltage and complex impedance measurements. Current flows from the aluminum through the polymer film to the ITO, and the diode will be forward biased when the aluminum electrode is connected to the negative terminal of the voltage source.

For the I-V measurement, the sample was placed in an HP 16055A text fixture which is interfaced with the HP 4140B PA meter / DC voltage source measuring device. The applied voltage was scanned between –3V and 3V.

5.3 Complex Impedance measurement

Impedance spectroscopy was measured with HP 4192A Low Frequency Impedance Analyzer together with a HP 16047A text fixture. The bias voltage applied to the sample ranged between –3V and 3V, in steps of 1V. For every bias voltage used, a sinusoidally oscillating voltage of V_{rms} = 10mV was applied. The

frequency was scanned between 500Hz and 10MHz for each bias. The Cole-Cole plots of the sandwich structure Al/PEOPT/ITO thus obtained were drawn as in Fig. 6.3 and analyzed. For the analysis of the complex impedance spectrum, a semicircular function is written using Microcal Origin and used as a non-linear curve fit.

6. Results and Discussions

6.1 Absorption spectrum

The optical absorption spectrum of PEOPT depicted in Fig. 6.1 shows that it absorbs electromagnetic radiation in the visible range. From the absorption curve the turn on occurs at a wavelength near 600nm. Using the relation $E_g = \frac{hc}{\lambda}$, the band gap E_g of PEOPT is calculated to be 2.07eV. From the fact that the energy gap for semiconductors falls in the range between 0.7eV and 3eV, PEOPT can be categorized as one of the semiconducting organic polymers.

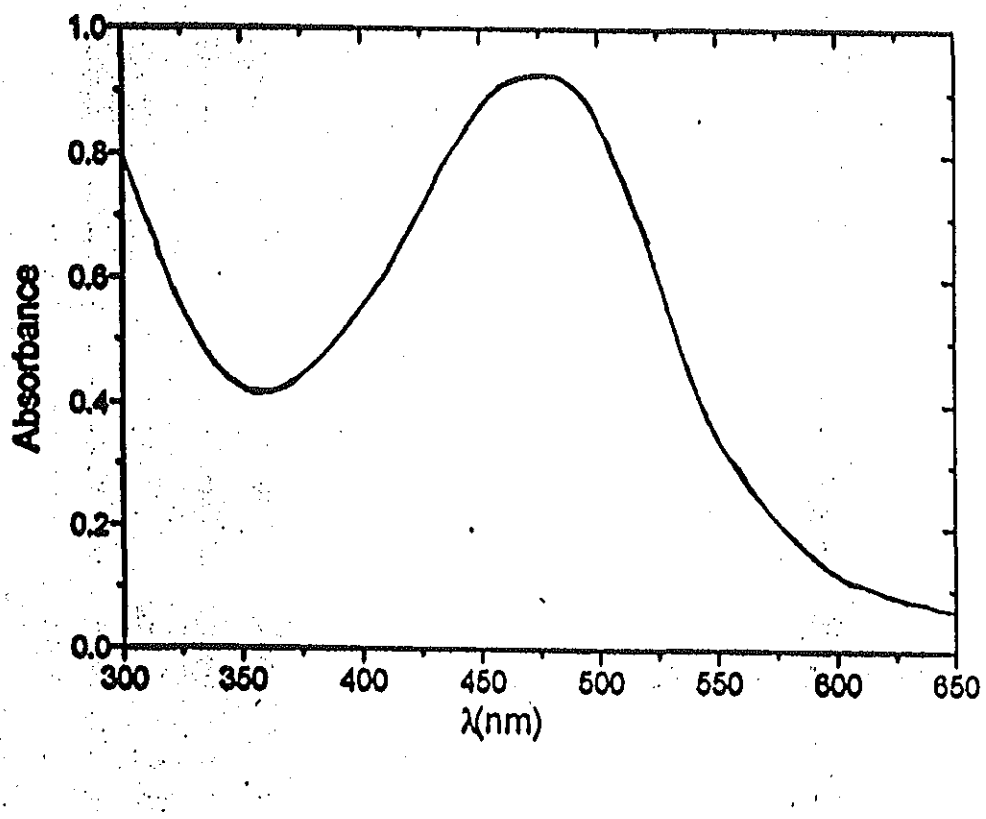

Fig. 6.1 Absorption spectrum of PEOPT

6.2 Current – voltage characteristics

The current–voltage curve of Al / PEOPT / ITO sandwich structure in the dark is asymmetric and non-ohmic, see Fig. (6.2a). There is an exponentially increasing region at a forward voltage. From the curve it is clear that the device shows rectification property in the dark with a turn on voltage at about 2V.

A semi-logarithmic plot of the current density (J) versus the applied voltage (V) plotted in Fig. (6.2b) shows an exponentially increasing current in the applied voltage region between 2V and 2.7V. This exponential dependence can be attributed to a formation of the depletion region near the Al / PEOPT interface.

In section (3.1) we have seen that p-type semiconductors form a rectifying barrier at the interface when the work function of the metal is less than that of a semiconductor. Thus, for PEOPT, which behaves as a p-type semiconductor, its work function is in between that of Al (4.25eV) and ITO (4.9eV).

The saturation current density, J_s, is obtained from the intercept of the linear plot of log(J) versus V curve with V = 0 axis, see Fig. (6.2c). From the intercept J_s is obtained to be 4.4×10^{-11} A/cm^2. Using this value and taking absolute temperature (T) to be room temperature, the potential barrier, ϕ_b, is calculated using eq. (3.3) to yield 1.0eV.

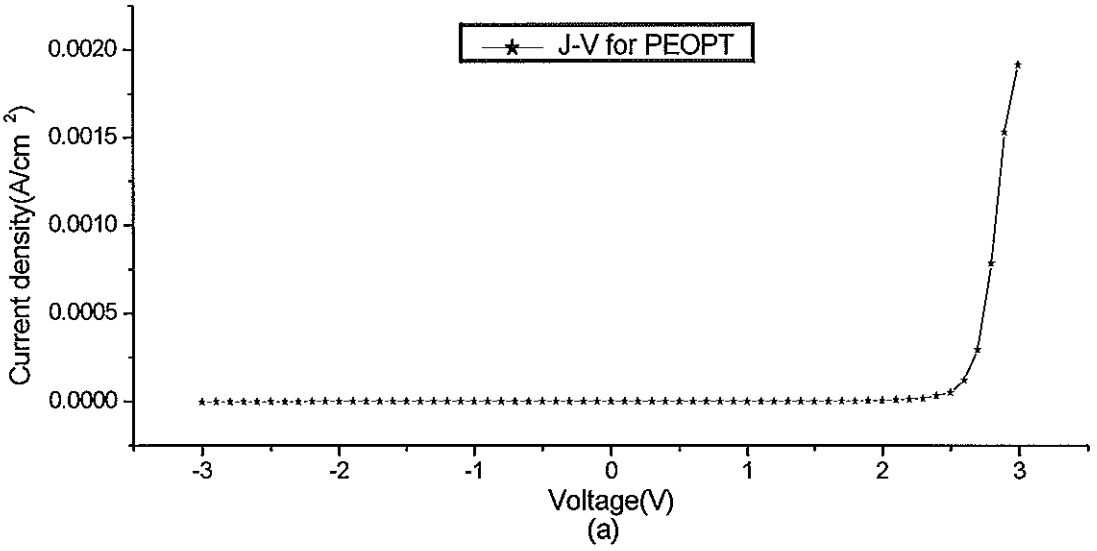
J-V for PEOPT
Current density(A/cm 2)
0.0020
0.0015
0.0010
0.0005
0.0000
-3
-2
-1
0
1
2
3
Voltage(V)
(a)

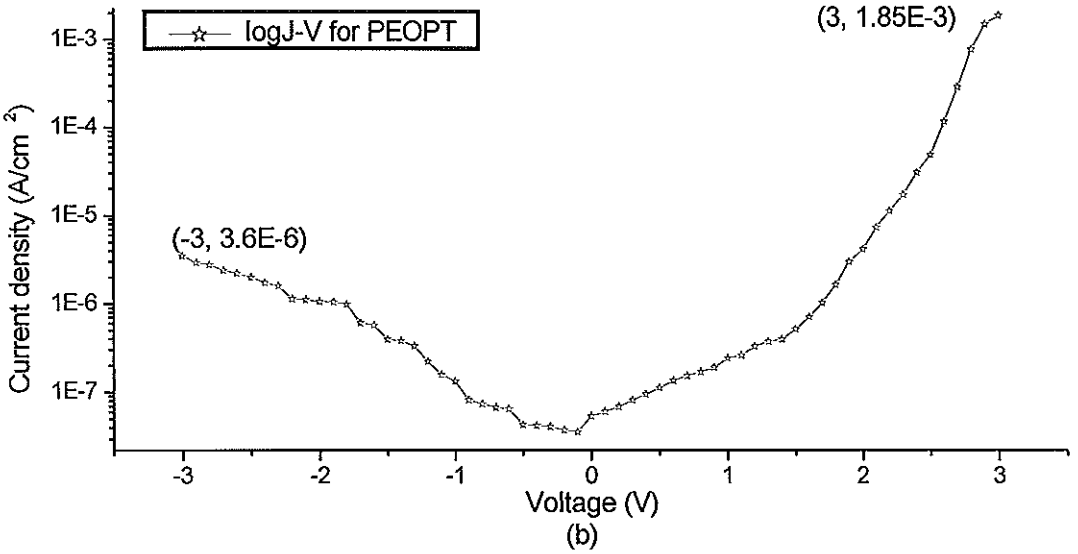
logJ-V for PEOPT
(3, 1.85E-3)
(-3, 3.6E-6)
Current density (A/cm 2)
1E-3
1E-4
1E-5
1E-6
1E-7
-3
-2
-1
0
1
2
3
Voltage (V)
(b)

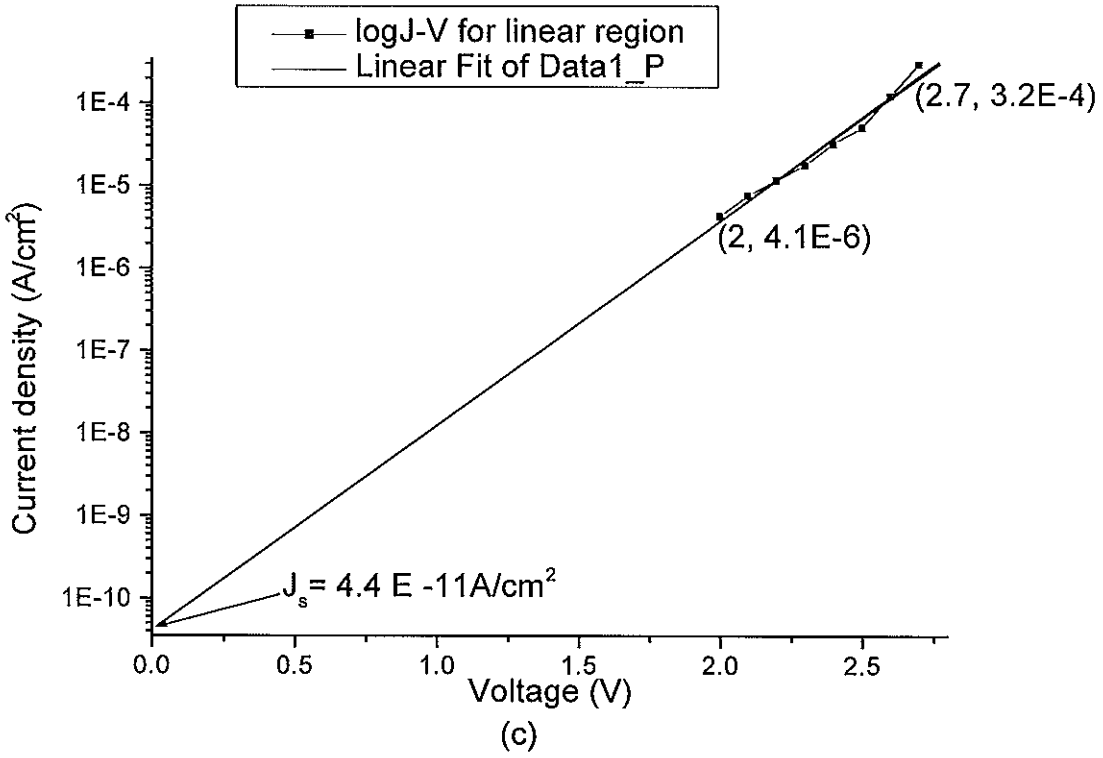

Fig. 6.2 (a) Current density (J)–voltage (V) characterstics, (b) logJ-V and (c) logJ-V for selected range of voltage, for PEOPT

The slope of the logarithmic plot is related to the quality factor n through the relation

$$\frac{1}{n} = \frac{kT}{q}\frac{\Delta \ln(J)}{\Delta V} \tag{6.1}$$

with the help of eq. (6.1), n is found to be 1.8. When n = 1, the Schottky barrier is ideal, whereas for higher values, e.g. $n \geq 2$, a mid-gap recombination of electrons and holes occurs.

Table 6.1 Parameters extracted from Fig. 6.2.

$J_s(A/cm^2)$	ϕ_b (eV)	n	γ
4.4×10^{-11}	1.0	1.8	510

The rectification ratio for the PEOPT can also be obtained from the log(J)-V curve by considering the current at the two extreme biasing voltages (-3V and 3V). From this consideration the rectification ratio γ is found to be about 510. Parameters extracted from Fig. (6.2) are listed in Table 6.1.

6.3 Complex impedance analysis

Information about the bulk resistance and the Schottky junction can be obtained by complex impedance measurements. Fig. (6.3) shows the impedance spectroscopy results as a function of frequency and selected applied voltages in the forward and reverse bias. The filled points in the figure are the measured coordinates of the real and imaginary components of the impedance.

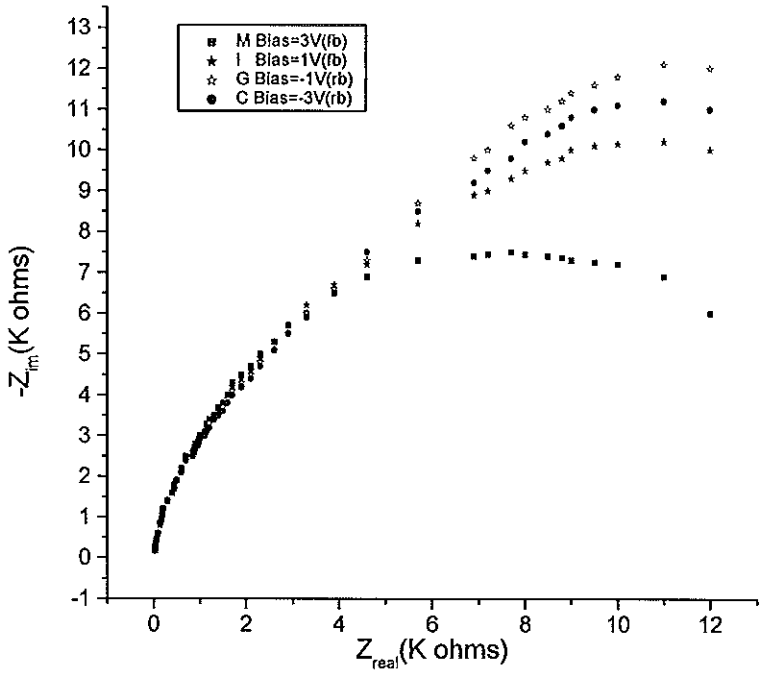

Fig. 6.3 Cole-Cole plot of Al/PEOPT/ITO sandwich structure

The impedance spectra consist of part of a single semicircle whose diameter corresponds to the resistance of the depletion region for the corresponding bias voltage. These semicircles are bias voltage dependent. Smaller bias voltage gives semicircles with larger diameter when extrapolated to the real impedance axis. Thus we can model our sample (Al / PEOPT / ITO) by one parallel RC circuit in series with the contact resistance, R_c. The contact resistance is the distance from the origin to the intersection of the semicircle with the real axis of the impedance plot corresponding to the highest frequency. The relation $-Z_{imag.} = (\omega c)^{-1}$ is used to estimate the value of the capacitance C.

The impedance spectra for different bias voltages and the corresponding circular fit are shown in Fig. 6.4.

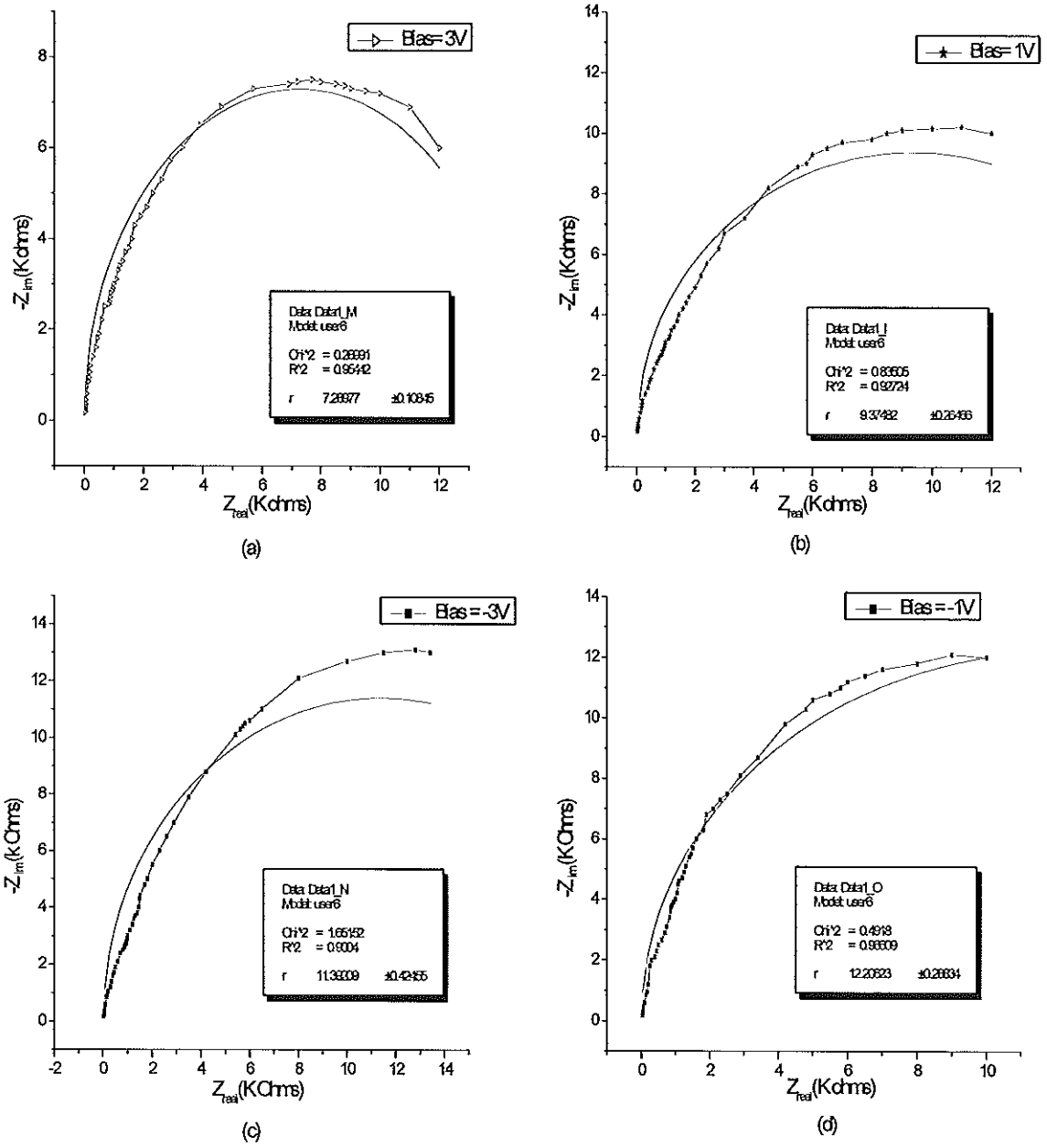

Fig. 6.4 Cole-Cole plots of different biasing voltage with their respective curve fits.

The Cole-Cole plot depicted in Fig. 6.3 and the current voltage characteristics shown in Fig. 6.2 are very consistent. For forward bias voltage the current is very high i.e., facing less resistance. The impedance curve shows less resistance (small semicircle) for forward bias voltage. The parameters obtained from the Cole-Cole plot of Fig. (6.3) are listed in Table 6.2.

Table 6.2 Parameters[a] obtained from Fig. 6.3

V_b (V)	R_c(ohm)	R(K ohm)	C(nF/cm^2)
3	30	14	440
1	30	18	340
-1	30	24	260
-3	30	22	280

a. R_c and R are series and depletion region resistances, respectively. The negative values of V_b are reverse bias voltages.

References:

1. L.H. Spirling, *Introduction to physical polymer science*, John Wiley & Sons, Inc. New York, 1986.
2. Siegmar Roth, *One-dimensional metals*, VCH Publishing, Inc., New York, NY, 1995.
3. Bantikassegn Workalemahu, *Ph.D Dissertation*, ISBN 91-7871-581-4, Linkoping University, Sweden, 1996.
4. D.M. Taylor and H.L. Gomes, *J.phys. D: Appl. Phys.*, **28** (1995) 2554.
5. G. Gustafsson, M. Sundberg, O. Inganas and C. Svensson, *J. Molecular Electronics*, **6** (1990) 105.
6. M. Granstrom, M. Berggren, O. Inganas, *Synth. Met.*, **76** (1996) 141.
7. O. Inganas, M. Berggren, M.R. Andersson, G. Gustafsson, T. Hjertberg, O. Wennerstrom, P. Dyreklev and M. Granstrom, *Synth., Meth.*, **71** (1994) 2121.
8. P. Dyreklev, M. Berggren, O. Inganas, M.R. Andersson, O. Wennerstrom and T. Hjertberg, *Adv., Mat.*, **7** (1995) 43.
9. M. Granstrom, M. Berggren, D. Pade, O. Inganas, M.R. Andersson, T. Hjertberg and O. Wennerstrom, *supramolecular Science*, **4** (1997) 27.
10. J.H. Burroughes, D.D.C. Bradley, A.R. Brown, R.N. Marks, K. Mackay, R.H. Friend, P.L. Burns & A.B. Holmes, *Nature*, **347** (1990) 539.
11. I.D. Parker, *J. Appl. Phys.*, **75** (1994) 1656.
12. D. Brawn and A.J. Heeger, *Appl. Phys. Lett.* **58** (18), (1991) 1982.

13. P. Dyreklev, G. Gustafsson, O. Inganas and H. Stubb, *Solid State Comm.*, **82** (1992) 317.

14. P. Dyreklev, O. Inganas, J. Paloheimo and H. Stubb, *J. Appl. Phy.*, **71** (1992) 2816.

15. Teketel Yohannes and O. Inganas, *Journal of Electrochemical Society*, **143** (1996) 2310.

16. H. Shirakawa, E.J. Louis, S.C. Gau and A.G. MacDiarmid, *Phy. Rev. Lett.*, **39** (1977) 1098.

17. H. Shirakawa, E.J. Louis, A.G. MacDiarmid, C.K. Chiang, and A.J. Heeger, *Chem. Commun.*, (1977) 578.

18. Robert J. Ouellette, *Organic Chemistry*, MacMillan, Pub. Co. (1994)

19. C. Kittel, *Int. to Solid State Physics*, 5th ed., Wiley Eastern Limited, (1976).

20. R.E. Peierls, *Quantum theory of solids*, Clarendon Press, Oxford, 1955.

21. N.J. Zabusky and M.D. Kruskal, *Phy. Rev. Lett.* **15** (1965) 240.

22. Yu. Lu, *Solitons and polarons in conducting polymers*, World Scientific Publishing Co. Pt. Ltd., (1988).

23. A.J. Heeger, S. Kivelson, J.R. Schrieffer, W. P. Su, *Rev. Mod. Phy.* **60** (1988) 781.

24. W. Bantikassegn, O. Inganas, *Thin solid Films*, **293** (1997) 138.

25. J.L. Bredas, J.C. Scott, K. Yakushi, and G.B. Street, *Phy. Rev.,* B **30** (1984) 1023.

26. R.R. Chance, J.L. Bredas and R. Silbey, *Phy. Rev.,* B **29** (1984) 4491.

41. W. Bantikassegn and O. Inganas, *Synth. Met.*, **87** (1997) 5.

42. I.H. Campbell, D.L. Smith and J.P. Ferraris, *Appl. Phys. Lett.*, **66** (22), (1995) 3030

43. Jovan Mijovic and F. Bellucci, *Trip* **4** (1996) 74.

44. J.R. MacDonald, ed., *Impedance spectroscopy*, Emphasizing Solid Materials and Systems, John Wiley & Sons, New York, (1987).

45. K.S. Cole and R.H. Cole, *J. Chem. Phy.*, **9** (1941) 341.

46. Wolfgang Demtroder, *Laser Spectroscopy* 2nd ed., Springer (1995).

47. L. S. Roman, W. Mammo, L. A.A. Petersson, M. R. Andersson, O. Inganas, *Adv. Mater.* **10** (1998).